

## Variogram analysis of magnetic and gravity data

Stefan Maus\*

### ABSTRACT

Model variograms describe the space domain statistics of magnetic and gravity data. Variogram analysis can be used to map intensity, depth, and scaling exponent (self-correlation) of source. In previous statistical methods the measured data were gridded and transformed to the wavenumber domain; then their power spectrum was analyzed using a spectral model. To avoid the loss and distortion of information during gridding and wavenumber domain transform, I transform the spectral model to the space domain instead. Variograms are the appropriate space domain counterparts of magnetic and gravity power spectra. The variogram of the field above a self-similar half-space model is governed by three parameters: intensity, depth, and scaling exponent. These source parameters can be mapped with high resolution and accuracy by fitting model variograms directly to magnetic and gravity line data variograms.

### INTRODUCTION

Density and susceptibility distributions in the earth's continental crust are self-similar (scaling, fractal), with a power spectrum  $P(\mathbf{k})$  proportional to  $|\mathbf{k}|^{-\beta}$ , where  $\mathbf{k}$  is the wavevector and  $\beta$  is the scaling exponent (Pilkington and Todoeschuck, 1990, 1993, 1995). Self-similar random functions were first proposed by Kolmogorov (1941, 1961) to model velocity fluctuations in a 3-D turbulent medium. Their importance for the earth sciences was discovered by Mandelbrot (1983).

The spectra of gravity and magnetic fields are related to the spectra of their respective source distributions (Naidu, 1968). Self-similar source models lead to realistic spectral models for gravity and magnetic data (Gregotski et al., 1991; Pilkington and Todoeschuck, 1993; Pilkington et al., 1994; Maus and Dimri, 1995b, 1996). Such models can play an important role in the processing and interpretation of potential field data (Maus 1996), for example, in gridding (Pilkington et al., 1994), susceptibility mapping (Gregotski et al., 1991), depth estimation

(Pilkington et al., 1994; Maus and Dimri, 1995a), and the computation of isostatic gravity residuals (Chapin, 1996).

In depth estimation by spectral analysis, magnetic data are interpolated to a regular grid and transformed by fast Fourier transform (FFT) to wavenumber domain; then their azimuthally averaged power spectrum is analyzed (Spector and Grant, 1970). However, even if the former spectral slope models are substituted by the more realistic self-similar models, depth from magnetic power spectra remains inaccurate (Maus and Dimri, 1996). This is because of the distorting effects of gridding, preparation for FFT, and azimuthal averaging on the data power spectra.

Here, I transform a self-similar spectral model analytically to the space domain to avoid the distorting effects of transforming measured data to the wavenumber domain. I argue that variograms are the appropriate space domain statistical models for analyzing magnetic and possibly gravity data.

After describing my spectral model for the magnetic field, I derive the corresponding variogram model for the complex case of aeromagnetic profiles in a nonvertical inducing field. The variogram model for gravity data is subsequently derived as a special case. Graphs of the model variograms illustrate the influence of profile orientation, depth, source intensity, and scaling exponent. Finally, a section on practical aspects proposes solutions to key difficulties in implementing a variogram analysis algorithm. A case study including further explanations and a comparison with Spector and Grant's method is published as a separate paper (Maus et al., 1999, this issue).

### SPECTRAL MODELS

#### Magnetic field power spectrum

Let us assume that magnetization at location  $\mathbf{r}$  can be expressed as the product of a scalar susceptibility  $\chi(\mathbf{r})$  and a constant geomagnetic field  $\mathbf{N}$ . This implies, in particular, that no significant component of remanent magnetization exists in any direction other than  $\mathbf{N}$ .

The power spectrum  $P_{\Delta T}(\mathbf{k})$  of the magnetic field  $\Delta T$  in a horizontal observation plane due to a slab of scaling sources can then be expressed [Maus et al., 1997, substituting

Manuscript received by the Editor September 24, 1996; revised manuscript received September 18, 1998.

\*Institut für Geophysik und Meteorologie der Technischen Universität Braunschweig, Mendelssohnstr. 3, 38106 Braunschweig, Germany. E-mail: smaas@gwdg.de.

© 1999 Society of Exploration Geophysicists. All rights reserved.

equations (16) and (19) in equation (14)] as

$$P_{\Delta T}(\mathbf{s}) = \frac{\mu_0^2}{4N^2} (n_z^2 + H^2 \cos^2 \theta)^2 s^2 \exp(-2sz) \times \int_{-\infty}^{\infty} [1 - \exp(-ts - itw) - \exp(-ts + itw) + \exp(-2ts)] (s^2 + w^2)^{-1} c_s (s^2 + w^2)^{-\beta/2} dw, \quad (1)$$

where  $\mathbf{s} = (u, v)$  is the horizontal wavevector,  $s = |\mathbf{s}|$ ,  $w$  is the vertical component of the wavevector,  $z$  is the distance between the observation plane and the top of the slab,  $t$  is the thickness of the slab,  $\mathbf{N} = (n_x, n_y, n_z)$  is the geomagnetic field,  $N = |\mathbf{N}|$  is its intensity,  $H = |(n_x, n_y)|$  is its horizontal intensity,  $\theta$  is the angle between  $\mathbf{s}$  and  $\mathbf{H}$ , and  $\mu_0$  is the magnetic permeability of free space. The parameters  $c_s$  and  $\beta$  refer to the susceptibility distribution  $\chi(\mathbf{r})$  on a full-space with power spectrum

$$P_\chi(u, v, w) = c_s (u^2 + v^2 + w^2)^{-\beta/2}, \quad (2)$$

of which the slab is a spatial subset. Hence, the slab is thought to be carved out of an imagined self-similar 3-D susceptibility distribution. Note that the slab in an otherwise empty space is neither self-similar nor does it have a power spectrum as in equation (2).

The limited depth extent of crustal magnetization has no noticeable effect on the power spectrum of the magnetic field up to wavelengths of about three times the depth to bottom (Maus et al., 1997). For most practical cases, where the size of the data analysis window is much smaller, we can simplify equation (1) by utilizing a half-space model, corresponding to  $t = \infty$ . Then

$$P_{\Delta T}(\mathbf{s}) = c_s \frac{\mu_0^2}{4N^2} (n_z^2 + H^2 \cos^2 \theta)^2 s^2 \exp(-2sz) \times \int_{-\infty}^{\infty} (s^2 + w^2)^{-\beta/2-1} dw \quad (3)$$

$$= c_s \frac{\mu_0^2}{4N^2} (n_z^2 + H^2 \cos^2 \theta)^2 s^{-\beta} \exp(-2sz) \times \int_{-\infty}^{\infty} [1 + (w/s)^2]^{-\beta/2-1} dw \quad (4)$$

$$= c_s \frac{\mu_0^2}{2N^2} (n_z^2 + H^2 \cos^2 \theta)^2 s^{-\beta+1} \exp(-2sz) \times \int_0^{\infty} [1 + a^2]^{-\beta/2-1} da, \quad (5)$$

with  $a = w/s$ . Solving the integral using Gradshteyn (1994, equation 3.251.2) gives

$$P_{\Delta T}(\mathbf{s}) = c_s \left( \frac{\mu_0}{2N} \right)^2 B[1/2, (\beta + 1)/2] \times \underbrace{(n_z^2 + H^2 \cos^2 \theta)^2}_{Dir(\theta)} \underbrace{s^{-\beta+1} \exp(-2sz)}_{Q(s)}, \quad (6)$$

where  $B$  is the beta function  $B(x, y) = \Gamma(x)\Gamma(y)/\Gamma(x + y)$ .

### Gravity field power spectrum

The spectrum  $P_g$  of the vertical derivative of the anomalous gravity potential from a self-similar density distribution within a half-space can be written (Naidu, 1968; Maus and Dimri, 1995b) as

$$P_g(\mathbf{s}) = c_s \frac{4\sigma^2}{\pi^2} \exp(-2sz) \int_{-\infty}^{\infty} (s^2 + w^2)^{-\beta/2-1} dw \quad (7)$$

$$= c_s \frac{4\sigma^2}{\pi^2} B[1/2, (\beta + 1)/2] s^{-\beta-1} \exp(-2sz), \quad (8)$$

where  $\sigma$  is the universal gravity constant and  $c_s$  and  $\beta$  are parameters describing the anomalous density distribution of a half-space model as in equation (2).

Comparing equations (6) and (8) shows that the gravity model is very similar to the  $\Delta T$  model for the special case of a vertical inducing field  $\mathbf{N} = (0, 0, N)$ .

### Scaling exponents

The 3-D scaling exponents of crustal susceptibility and density can be inferred from 1-D and 2-D cross-sections, such as bore wells and surveys at the surface. Furthermore, they can be derived from the respective magnetic and gravity fields. Relationships between the scaling exponents of a field and its sources in different dimensions have been derived by Maus and Dimri (1994).

Marine gravity off Norway and south of Japan, as well as free air and Bouguer gravity of the former Soviet Union, have a consistent  $\beta$  of 3.5 (Maus et al., 1998). Pilkington and Todoeschuck (1990) derive scaling exponents of around one, corresponding to  $\beta \approx 3$  from density logs.

Gregotski et al. (1991) estimate scaling exponents from eight aeromagnetic data sets, finding values in the range of 2.8 to 3.4 corresponding to  $3.8 < \beta < 4.4$ . An average scaling exponent of  $\beta = 4$  is further confirmed by Pilkington and Todoeschuck (1993, 1995) from susceptibility logs, aeromagnetic data, and susceptibility surveys. In contrast, Maus and Dimri (1995b) derive scaling exponents of  $\beta < 3$  from helicopter magnetic data and a 4-km vertical rock susceptibility profile at the German Continental Deep Drilling site.

In general, density logs are smoother than susceptibility logs. The scaling exponent of density should therefore be higher than that of susceptibility—at least on a local scale.

### SPACE DOMAIN COUNTERPARTS

#### ACF versus variogram

The most obvious space domain counterpart of a power spectrum is the auto-correlation function (ACF),

$$ACF(\boldsymbol{\tau}) = \langle X(\mathbf{r} + \boldsymbol{\tau})X(\mathbf{r}) \rangle, \quad (9)$$

which is related to the power spectrum by a Fourier transform,

$$ACF(\boldsymbol{\tau}) = \int_{-\infty}^{\infty} \int_{-\infty}^{\infty} \exp(i\boldsymbol{\tau} \cdot \mathbf{s}) P(\mathbf{s}) du dv. \quad (10)$$

However, if we use equation (10) to derive the ACF counterpart of the spectral model defined by equation (6), the integrals do not converge for  $\beta > 3$ . This reflects the fact that for  $\beta > 3$ , equation (6) describes an inhomogeneous random

function (equivalent to a nonstationary process in one dimension) with infinite variance and a variable mean value. This is not just a mathematical problem. Anyone having attempted to estimate an ACF from magnetic data must have faced the difficulty of estimating the baseline, i.e., estimating  $ACF(0)$ . Thus, the ACF is an inappropriate device for statistical characterization of  $\Delta T$  magnetic data.

For  $3 < \beta < 5$ , equation (6) describes a random function that belongs to the class of locally homogeneous random functions (corresponding to processes with stationary increments in one dimension). For these, the difference between two values, measured at a constant vector separation, is stationary. A locally homogeneous random function is characterized by its variogram (Cressie, 1993),

$$V(\boldsymbol{\tau}) = \langle [X(\mathbf{r}) - X(\mathbf{r} + \boldsymbol{\tau})]^2 \rangle. \quad (11)$$

This variogram has a spectral representation (Yaglom, 1986, 435),

$$V(\boldsymbol{\tau}) = \int_{-\infty}^{\infty} \int_{-\infty}^{\infty} [1 - \cos(\boldsymbol{\tau} \cdot \mathbf{s})] P(\mathbf{s}) du dv. \quad (12)$$

For the magnetic model of equation (6), the integrals in equation (12) converge for  $\beta < 5$  (see below). Thus, the variogram is applicable to a wider and more realistic range of scaling exponents than the ACF.

Whether it is better to utilize the ACF or the variogram to characterize the statistics of measured data is an important question. To further illustrate the problem, let us consider the  $\Delta T$  measurements along an aeromagnetic profile as a 1-D random process. One can estimate the variogram of this process using equation (11). The ACF can then be derived from the variogram using the relationship (Yaglom, 1986)

$$ACF(\tau) = 1/2[V(\infty) - V(\tau)]. \quad (13)$$

However, to be able to use this relationship, the variogram must level off to a constant value for a lag  $\tau$  smaller than the window size. Otherwise,  $V(\infty)$  remains unknown. This is exactly where the problem lies. Variograms of  $\Delta T$  data tend to keep increasing, even for large lags.

Generally speaking, the use of variograms instead of ACFs in the interpretation of  $\Delta T$  magnetic data—and probably gravity data as well—makes sense both from a theoretical and a practical point of view.

### Magnetic variogram

Let us introduce polar coordinates  $(s, \phi)$  in the 2-D wave-number domain of the observation plane. We are interested in changes of lag  $\tau$  along profiles with a constant direction. Let us choose the coordinate system in such a way that  $\phi = 0$  for this direction. Then the scalar product  $\boldsymbol{\tau} \cdot \mathbf{k}$  in equations (10) and (12) reduces to  $\tau s \cos \phi$  and we can write equation (12) as

$$V(\tau) = \int_0^{\infty} \int_0^{2\pi} [1 - \cos(\tau s \cos \phi)] P_{\Delta T}(s, \phi) d\phi s ds, \quad (14)$$

where  $P_{\Delta T}(s, \phi)$  is the power spectrum defined by equation (6) in horizontal polar coordinates. If the integrals converge, the right-hand side of equation (14) is well defined, and we obtain

a space domain model for the variogram of measured profiles with a constant direction.

Denoting the declination of the normal field  $\mathbf{N}$  in terms of our new coordinate system ( $x$ -axis parallel to the profiles) by  $\alpha$ , we obtain  $\theta = \phi - \alpha$ . Here,  $\phi$  is the angle between the wavevector and the profiles and  $\theta$  is the angle between the wavevector and the horizontal component of  $\mathbf{N}$  [see also the text following equation (1)]. Then equation (14) can be written as

$$V(\tau) = c_s \left( \frac{\mu_0}{2N} \right)^2 B[1/2, (\beta + 1)/2] \int_0^{\infty} \int_0^{2\pi} [1 - \cos(\tau s \cos \phi)] Dir(\phi - \alpha) d\phi Q(s) s ds. \quad (15)$$

To solve the inner, angular integral in equation (15),

$$I_{angular}(\tau s) = \int_0^{2\pi} [1 - \cos(\tau s \cos \phi)] Dir(\phi - \alpha) d\phi, \quad (16)$$

the term  $Dir(\phi - \alpha)$  defined in equation (6) can be expressed in terms of powers of  $\sin \phi$ :

$$Dir(\phi - \alpha) = \{n_z^2 + H^2[\cos(\phi - \alpha)]^2\}^2 \quad (17)$$

$$= \{n_z^2 + H^2[\cos \phi \cos \alpha + \sin \phi \sin \alpha]^2\}^2 \quad (18)$$

$$= [n_z^2 + (n_x \cos \phi + n_y \sin \phi)^2]^2 \quad (19)$$

$$\begin{aligned} &= (n_y^4 - 6n_y^2 n_x^2 + n_x^4) \sin^4 \phi \\ &\quad + (4n_x n_y^3 - 4n_y n_x^3) \cos \phi \sin^3 \phi \\ &\quad + (6n_y^2 n_x^2 + 2n_y^2 n_z^2 - 2n_x^4 - 2n_x^2 n_z^2) \sin^2 \phi \\ &\quad + (4n_y n_x n_z^2 + 4n_y n_x^3) \cos \phi \sin \phi \\ &\quad + n_z^4 + n_x^4 + 2n_z^2 n_x^2 \end{aligned} \quad (20)$$

$$\begin{aligned} &=: T_4 \sin^4 \phi + T_3 \cos \phi \sin^3 \phi + T_2 \sin^2 \phi \\ &\quad + T_1 \cos \phi \sin \phi + T_0, \end{aligned} \quad (21)$$

where  $=:$  denotes the definition of  $T_0, \dots, T_4$ . The inner integral  $I_{angular}(\tau s)$  of equation (16) can then be written as

$$\begin{aligned} I_{angular}(\tau s) &= \int_0^{2\pi} [1 - \cos(\tau s \cos \phi)] \\ &\quad \times (T_4 \sin^4 \phi + T_3 \cos \phi \sin^3 \phi \\ &\quad + T_2 \sin^2 \phi + T_1 \cos \phi \sin \phi + T_0) d\phi \end{aligned} \quad (22)$$

$$\begin{aligned} &= 4 \int_0^{\pi/2} [1 - \cos(\tau s \cos \phi)] \\ &\quad \times (T_4 \sin^4 \phi + T_2 \sin^2 \phi + T_0) d\phi. \end{aligned} \quad (23)$$

This integral can be solved using Bessel functions  $J_n$  of integer order  $n$  (Gradshteyn and Ryzhik, 1994, equation 4.411.4),

$$J_n(x) = \frac{2(x/2)^n}{\sqrt{\pi} \Gamma(n + 1/2)} \int_0^{\pi/2} \cos(x \cos \phi) \sin^{2n} \phi d\phi, \quad (24)$$

where  $\Gamma$  is the gamma function, and the formulas

$$\int_0^{\pi/2} \sin^m \phi \, d\phi = \frac{\Gamma[(m+1)/2]\sqrt{\pi}}{2\Gamma[(m+2)/2]}, \quad (25)$$

$$\Gamma(1/2) = \sqrt{\pi}, \quad (26)$$

and

$$\Gamma(x+1) = x\Gamma(x). \quad (27)$$

Equation (23) then becomes

$$I_{angular}(\tau s)/\pi = 2T_0 - 2T_0J_0(\tau s) + T_2 - \frac{2T_2}{\tau s}J_1(\tau s) + \frac{3}{4}T_4 - \frac{6T_4}{\tau^2s^2}J_2(\tau s). \quad (28)$$

With equation (15) we obtain the final equation:

$$V(\tau) = \pi c_s \left( \frac{\mu_0}{2N} \right)^2 B[1/2, (\beta+1)/2] \times \int_0^\infty \left[ T - 2T_0J_0(\tau s) - \frac{2T_2}{\tau s}J_1(\tau s) - \frac{6T_4}{\tau^2s^2}J_2(\tau s) \right] e^{-2zs} s^{2-\beta} ds, \quad (29)$$

$$T = \frac{3}{4}(n_y^2 + n_x^2)^2 + 2n_z^2(n_y^2 + n_x^2 + n_z^2) \quad (30)$$

$$= \frac{3}{4}H^4 + 2n_z^2N^2, \quad (31)$$

$$T_0 = n_z^4 + n_x^4 + 2n_z^2n_x^2, \quad (32)$$

$$T_2 = 6n_y^2n_x^2 + 2n_y^2n_z^2 - 2n_x^4 - 2n_x^2n_z^2, \quad (33)$$

and

$$T_4 = n_y^4 - 6n_y^2n_x^2 + n_x^4. \quad (34)$$

Here,  $\mathbf{N} = (n_x, n_y, n_z)$  is expressed in coordinates relative to the flight lines. Since only even powers of  $n_x, n_y,$  and  $n_z$  appear, we need not take care of the orientation of the coordinate system as long as  $n_y = 0$  for  $\mathbf{H}$  parallel to the profiles and  $n_x = 0$  for  $\mathbf{H}$  perpendicular to the direction of the profiles.

### Gravity variogram

The gravity spectrum of equation (8) is very similar to, and somewhat simpler than, the magnetic spectrum of equation (6). The corresponding variogram model for  $g_z$  gravity data can be obtained from equation (29) as the special case of  $n_x = n_y = 0$  and  $n_z = 1$ . Further substituting  $-\beta$  for  $2 - \beta$  and adjusting the constants provides

$$V(\tau) = \frac{8\sigma^2c_s}{\pi} B[1/2, (\beta+1)/2] \times \int_0^\infty [1 - J_0(\tau s)] e^{-2zs} s^{-\beta} ds. \quad (35)$$

In this case, the variogram is horizontally isotropic. Consequently, the model is applicable to any set of gravity measurements located in a horizontal observation plane, whereas equation (29) requires the magnetic measurements to be located on a profile with constant direction.

### Convergence of the integrals in equations (29) and (35)

The variogram models of equations (29) and (35) are defined only for a limited range of scaling exponents. Using the relationship (Yaglom, 1986, 355)

$$\frac{J_{(n-2)/2}}{x^{(n-2)/2}} = \frac{2^{(2-n)/2}}{\Gamma(n/2)} \left[ 1 - \frac{x^2}{2n} + \frac{x^4}{2 \cdot 4n(n+2)} - \dots \right] \quad \text{for } n = 2, 3, \dots, \quad (36)$$

it can be shown that the integral in equation (29) converges in the interval  $s \in (0, 1]$  for  $\beta < 5$  and any  $z$ . In the remaining interval  $s \in (1, \infty)$ , the integral converges always if  $z > 0$ . In case  $z = 0$ , however, the integral converges only for  $\beta > 3$ . This latter restriction is probably of little practical consequence, since a small distance between the sources and the observation plane can always be assumed. The restrictions for the gravity variogram can be found by a similar line of reasoning.

In summary, the magnetic variogram (29) exists for  $\beta < 5$ , while the gravity variogram (35) exists for  $\beta < 3$ .

### Limitations

The statistical model developed here has the following known limitations:

- 1) It does not account for components of remanent magnetization perpendicular to the normal magnetic field.
- 2) It does not account for anomalies caused by topography. In particular, topographic gravity anomalies are often stronger than gravity anomalies caused by subsurface density variations.
- 3) It is based on the simplifying assumption that measurements are located in a horizontal plane, whereas ground and even airborne surveys usually follow surface topography.
- 4) Within a particular data analysis window, the source parameters  $z, \beta,$  and  $c_s$  are assumed to be constant. Hence, variations in  $z, \beta,$  and  $c_s$  can be detected only if their wavelength is larger than the size of the analysis window.
- 5) The case of multiple source layers is not considered.
- 6) For a susceptibility distribution with  $\beta < 3$ , the model does not provide for the variogram of the magnetic field at ground level because of a diverging integral in equation (29).
- 7) A density distribution with  $\beta \geq 3$  leads to a diverging integral in equation (35).
- 8) The integral in equation (29) must be evaluated numerically. Equation (35) has an analytical solution (personal communication, Peter Weidelt, 1995).

### GRAPHS OF THE VARIOGRAM

Some special cases of the variograms  $V$  defined by equation (29) and  $V_y$  defined later in equation (49) shall now be illustrated. In particular, the effect of the model parameters  $\mathbf{N}, c_s, z,$  and  $\gamma$  on the graphs of the variograms are demonstrated. For compatibility between the  $\Delta T$  and  $g_z$  spectral models given by equations (29) and (35), let us introduce  $\gamma$  as the 2-D scaling exponents of the fields in the horizontal observation plane, related to the scaling exponents of their 3-D source distributions by  $\gamma_{\Delta T} = \beta_{sus} - 1$  and  $\gamma_g = \beta_{dens} + 1$ , respectively (see also Maus and Dimri, 1994).

**Orientation of the profiles relative to N**

The parameter  $N$  is determined by the orientation of the measured profiles with regard to the direction and intensity of the earth's normal magnetic field. It is not a variable model parameter. Figures 1 and 2 show the model variograms  $V$  and  $V_y$  for different orientations of the profiles near the magnetic equator ( $n_z = 0$ ), where the effect of profile orientation is greatest. The variations are least for profiles perpendicular to the geomagnetic field and strongest for profiles parallel to the field. At higher geographic latitudes the anisotropy of the variations of the magnetic field is less pronounced. Figure 3 demonstrates that the variograms differ not only in amplitude but also in shape.

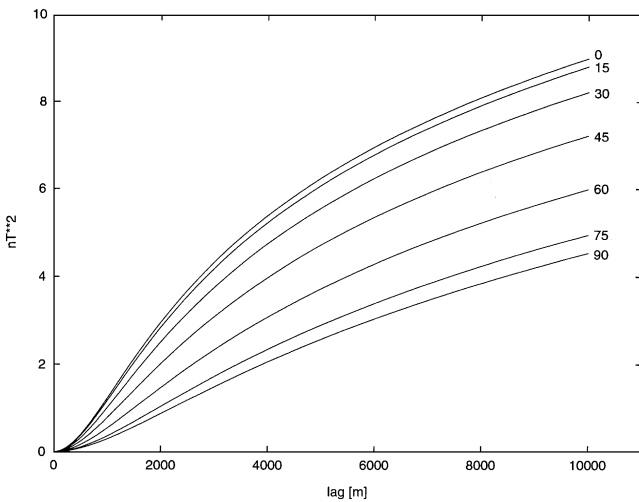


FIG. 1. Effect of the profile orientation relative to the horizontal component of the magnetic field  $H$ . Displayed are the model variograms  $V$  of equation (29) for different profile azimuth angles with  $z = 500$  m,  $\gamma = 2$ , and  $n_z = 0$ , hence at the magnetic equator where the effect of profile orientation is strongest.

**Intensity of the variations  $c_s$**

The parameter  $c_s$  may be of considerable practical interest since it reflects the intensity of source variations. For magnetic data, the square root of  $c_s$  is possibly related to the magnetization of the source rocks. On the graph of the variogram, however, the parameter  $c_s$  acts only as a constant factor.

**Depth to source  $z$**

The effect of depth to source  $z$  on the variogram  $V$  of equation (29) is displayed in Figure 4. With increasing depth to source, the variogram of the potential field experiences a drastic decrease in overall amplitude. However, this overall amplitude is already covered by the intensity parameter  $c_s$ . To estimate depth from variogram amplitude, we would have to assume  $c_s = \text{constant}$ . In general, this assumption is too strong,

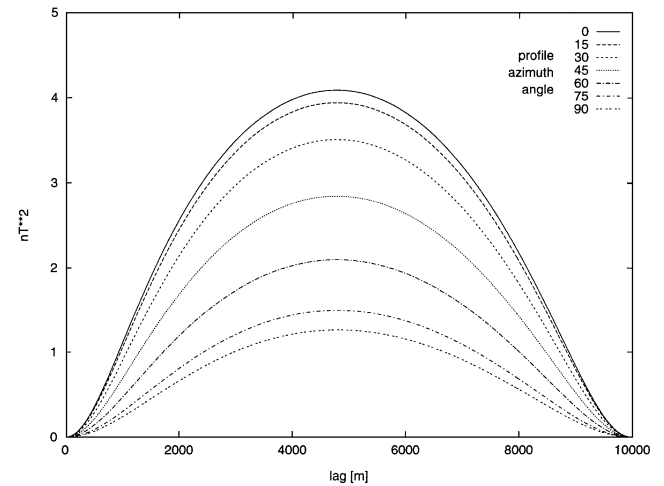


FIG. 2. Effect of the profile orientation on the modified model variograms  $V_y$  of equation (49) for different profile azimuth angles with  $z = 500$  m,  $\gamma = 2$ , and  $n_z = 0$ , same case as in Figure 1.

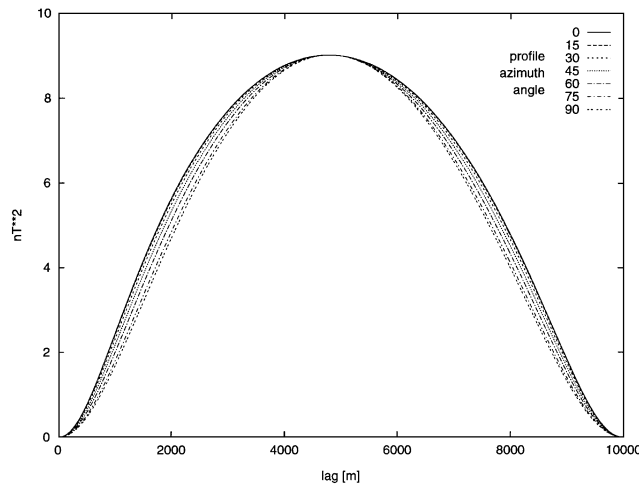


FIG. 3. Variograms  $V_y$  of Figure 2 rescaled to have equal amplitude at lag = 5 km. The variograms for different profile azimuth angles differ in amplitude as well as in shape.

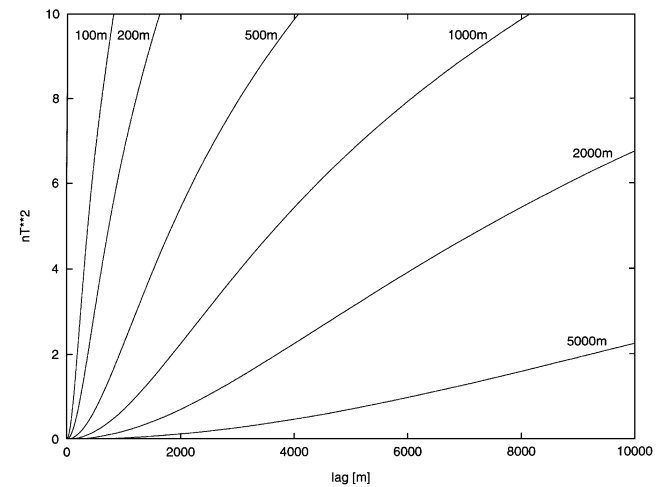


FIG. 4. Effect of the depth to source. Displayed are variograms  $V$  of equation (29) for  $\gamma = 2$ .

and it is advisable to keep  $c_s$  variable. If  $c_s$  is kept variable, then depth must be detected solely from differences in variogram shape.

Differences in shape of the modified variogram  $V_y$  due to depth are illustrated in Figure 5. Since upward continuation suppresses variations of short wavelength stronger than variations of long wavelength, variogram shape differs primarily at short lags. While there is a significant difference between the variograms for 1000 and 2000 m depth, the difference at 5000 m depth is negligible. Hence, the maximum resolvable depth is approximately one-fifth of the variogram length. From my experience, the window size must be at least twice the length of the variogram to be estimated. Therefore, a variogram estimated from a given window can resolve depths to not more than one-tenth of the window size. The exact ratio depends on further

factors, such as the scaling exponent of the source distribution. The smaller the  $\beta$ , the better the resolution of depth.

**Scaling exponent  $\gamma$**

The scaling exponent  $\gamma$  determines whether the variogram  $V$  (Figure 6) is generally convex or concave, i.e., whether it turns upward ( $\gamma > 3$ ) or toward higher lags ( $\gamma < 3$ ). The scaling exponent influences the shape of the variograms in a similar way as the depth to source. Compare Figure 6 with Figure 4 for  $V$  and Figure 7 with Figure 5 for  $V_y$ . This means that if we observe a smooth magnetic field, it can be caused either by a rugged source distribution (small  $\beta$ ) at a greater depth or by a smoother source distribution (larger  $\beta$ ) at a shallower depth. A consequence of this ambiguity is that  $\beta$  and  $z$  cannot be

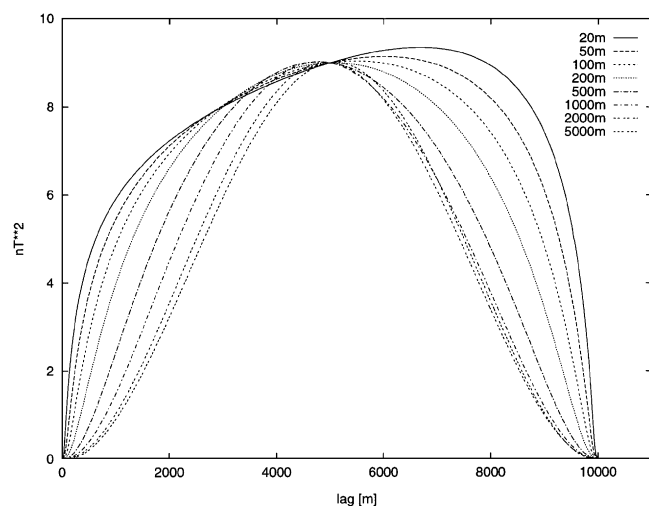


FIG. 5. Effect of the depth to source on the variograms  $V_y$  of equation (49) for  $\gamma = 2$ . Variograms are rescaled to intersect at 5 km lag.

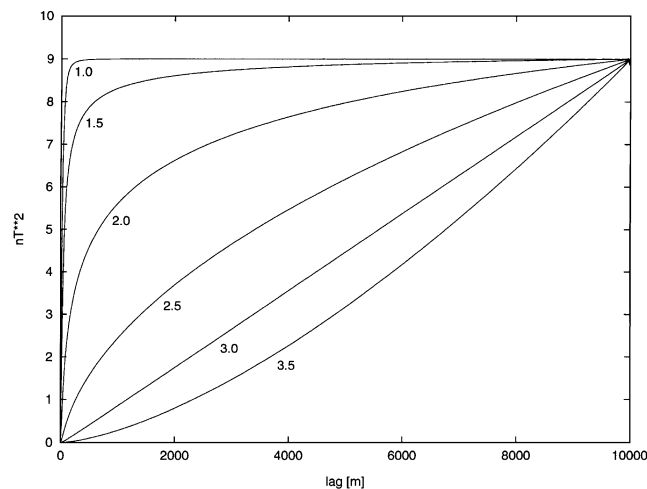


FIG. 6. Effect of the scaling exponent  $\gamma$  on the variograms  $V$  of equation (29) for  $z = 10$  m. The curves are rescaled to intersect at  $\tau = 10$  km. The depth  $z$  was chosen greater than zero; otherwise, the integral in equation (29) would not converge for the variograms with  $\gamma < 2$ .

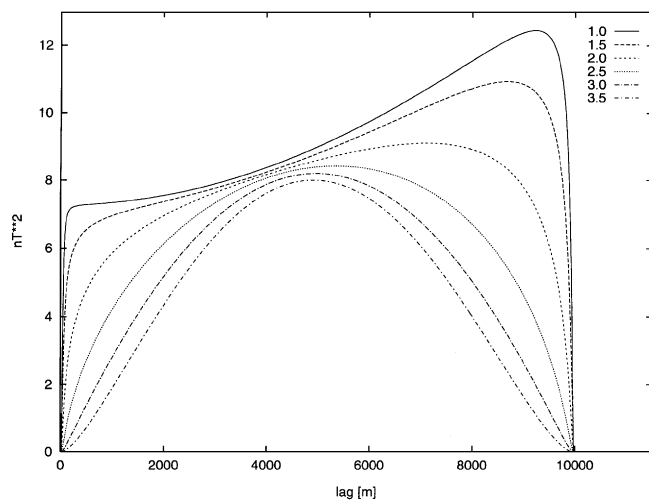


FIG. 7. Effect of the scaling exponent  $\gamma$  on the variograms  $V_y$  of equation (49) for  $z = 10$  m. Variograms are rescaled for better comparison. The scaling exponent influences the shape of the variogram in a similar but not identical way as the depth to source (see Figure 5).

resolved simultaneously unless, perhaps, by using very large windows.

### PRACTICAL ASPECTS

Following are some additional formulas that are essential in applying the variogram analysis method to real magnetic data sets.

#### Computing the model variogram

To compute the model variogram defined by equation (29) for a given set of model parameters, we have to numerically approximate the integral. At first glance this looks like a technical problem that could be solved by quadrature algorithms available in standard math software packages. However, the term in square brackets tends toward zero for low values of  $s$ , whereas  $s^{2-\beta}$  tends to infinity. The product of the two terms tends to zero for  $\beta < 4$  and to infinity for  $\beta > 4$ . To integrate numerically over this product can lead to arbitrary results.

A solution to the problem is the following: We use equation (36) with  $x = \tau s$  to approximate the Bessel functions in equation (29). For small values of  $\tau s$ , say,  $\tau s$  smaller than some  $a$ , it is sufficient to consider just the first two terms in equation (36). Since this approximation only holds for small  $\tau s$ , we split the integral in equation (29) into two parts:

$$V(\tau) = \int_0^\infty \dots = \int_0^{a/\tau} \dots + \int_{a/\tau}^\infty \dots =: V_1(\tau, a) + V_2(\tau, a). \quad (37)$$

The second integral  $V_2(\tau, a)$  is straightforward and can be evaluated with a standard quadrature algorithm. For the first integral, we use the first two terms in the square brackets of equation (36). Substituting  $T = 2T_0 + T_2 + (3/4)T_4$  in equation (29), we arrive at

$$V_1(\tau, a) = \pi c_s \left( \frac{\mu_0}{2N} \right)^2 B[1/2, (\beta + 1)/2] \times \left[ 2T_0 + \frac{T_2}{2} + \frac{T_4}{4} \right] \frac{\tau^2}{4} \int_0^{a/\tau} s^{4-\beta} e^{-2zs} ds. \quad (38)$$

The integral can now be solved using the relationship

$$\int_0^u x^{v-1} e^{-\mu x} dx = \mu^{-v} \Gamma_{incompl}(v, \mu u), \quad (39)$$

where  $\Gamma_{incompl}$  is the incomplete  $\Gamma$ -function, leading to

$$V_1(\tau, a) = \pi c_s \left( \frac{\mu_0}{2N} \right)^2 B[1/2, (\beta + 1)/2] \times \left[ 2T_0 + \frac{T_2}{2} + \frac{T_4}{4} \right] 2^{\beta-7} z^{\beta-5} \times \Gamma_{incompl} \left( 5 - \beta, \frac{2za}{\tau} \right) \tau^2. \quad (40)$$

Adding the two parts  $V_1$  and  $V_2$  according to equation (37) then yields the desired model variogram  $V(\tau)$ .

#### Estimating the variogram from a segment of a profile

In practice, we want to obtain the best possible estimate from the shortest possible segment of the profile. This can be achieved by utilizing the estimator

$$\hat{V}(\tau) = \frac{1}{T - \tau} \int_0^{T-\tau} [X(t + \tau) - X(t)]^2 dt, \quad (41)$$

where  $X(t)$  is the measured field, with  $X(0)$  and  $X(T)$  at the beginning and end of the segment, respectively. The value  $\hat{V}$  is a variogram estimated from measured data.

#### Extended model accounting for linear trends

The model variogram defined by equation (29) is the theoretical variogram of the magnetic field attributed to a horizontally infinite half-space of scaling sources. In practice, however, we are interested only in source parameters within a limited area (window). Furthermore, we want to keep this window as small as possible to enhance spatial resolution. Regarding small segments of a measured profile, one often finds a strong linear trend. This trend usually reflects large-scale geological features that are unrelated to the local magnetization. Such large-scale trends are expected for nonstationary data and are consistent with the variogram models of equations (29) and (35). However, equations (11) and (41) show that a linear trend in the data has a dramatic effect on the shape of the estimated variogram. To focus the analysis on the current data analysis window, linear trends in the data must be dealt with. Arguably, this is the key problem in designing a reliable variogram analysis algorithm.

It may appear that the obvious solution is to detrend a segment in the usual way—namely, fit a straight line in a least-squares sense, subtract it from the data, estimate the variogram from the detrended segment, and compare it with the model variograms of equations (29) or (35). However, the linear trends are an integral part of these model variograms. Strictly speaking, the model variograms of equations (29) and (35) do not apply to detrended data. One could ignore this problem and hope that detrending will just lead to lower model scaling exponents. However, this is far from obvious.

A clean solution is not only to detrend the data but also to modify the model variograms to account for the detrending. By the least-squares method of detrending, the data variograms are altered in a way that I am unable to quantify. In the following, I therefore use the more primitive method of fitting a straight line through the end points of the segment. For this detrending, the modified model variograms can be found as follows.

Let us denote the measured data within the considered segment of the profile by  $X(t)$ . Let us further denote the beginning of this segment by  $t = 0$  and the end by  $t = T$ , and let us subtract an offset from the data so that  $X(0) = 0$ . Then we can define a process  $Y(t)$ , which is derived from  $X(t)$  by

$$Y(t) := X(t) - \frac{t}{T} X(T). \quad (42)$$

The new process  $Y(t)$  has the advantage that the presumed linear trend in  $X(t)$  is not reflected in  $Y(t)$ . The variogram of  $Y(t)$  can be estimated from the measured data using equation (41). We have a model variogram  $V(\tau)$  defined by equation (29) for the process  $X(t)$  from which we now derive the model

variogram for  $Y(t)$ . The idea behind the following derivation is to answer the question, “If we have a variogram model  $V(\tau)$  for the process  $X(t)$ , what is the expected variogram  $\langle V_y(\tau) \rangle$  for the detrended process  $Y(t)$ ?” Using triangular brackets  $\langle \cdot \rangle$  for the expected value, equation (41) gives

$$\langle \hat{V}_y(\tau) \rangle = \left\langle \frac{1}{T-\tau} \int_0^{T-\tau} [Y(t+\tau) - Y(t)]^2 dt \right\rangle \quad (43)$$

$$= \left\langle \frac{1}{T-\tau} \int_0^{T-\tau} \left\{ \frac{\tau}{T} X(T) - [X(t+\tau) - X(t)] \right\}^2 dt \right\rangle \quad (44)$$

$$= \left\langle \frac{\tau^2}{(T-\tau)T^2} \int_0^{T-\tau} X(T)^2 dt \right\rangle + \left\langle \frac{1}{T-\tau} \int_0^{T-\tau} [X(t+\tau) - X(t)]^2 - \frac{2\tau}{T} X(T)X(t+\tau) + \frac{2\tau}{T} X(T)X(t) dt \right\rangle \quad (45)$$

$$= \frac{\tau^2}{T^2} V(T) + V(\tau) - \frac{1}{T-\tau} \int_0^{T-\tau} \times \frac{2\tau}{T} \langle X(T)X(t+\tau) \rangle - \frac{2\tau}{T} \langle X(T)X(t) \rangle dt \quad (46)$$

Since  $X(t)=0$  for  $t=0$ , the identity (Yaglom, 1986, equations 4.222 and 4.224)

$$\langle [X(t+\tau_1) - X(t)][X(t+\tau_2) - X(t)] \rangle = \frac{1}{2} [V(\tau_1) + V(\tau_2) - V(|\tau_1 - \tau_2|)] \quad (47)$$

reduces to

$$\langle X(\tau_1)X(\tau_2) \rangle = \frac{1}{2} [V(\tau_1) + V(\tau_2) - V(|\tau_1 - \tau_2|)] \quad (48)$$

so that

$$\langle V_y(\tau) \rangle = V(\tau) + \frac{\tau^2}{T^2} V(T) - \frac{\tau}{T(T-\tau)} \int_0^{T-\tau} V(t+\tau) - V(t) + V(T-t) - V(T-t-\tau) dt. \quad (49)$$

Equation (49) describes how the model variogram  $V(\tau)$  of the original segment  $X(t)$  can be transformed into a model variogram  $V_y(\tau)$  for the detrended segment  $Y(t)$ .

Generally speaking, it is essential to detrend a segment prior to estimating its variogram. The least-squares method provides a better estimate of trend, but the model variograms for the detrended process may be difficult to compute. For end-point detrending the effect on the model variograms is described by equation (49). Unfortunately, the end points are not always a good estimate of trend. Consider, for example, a prominent dike across-line at one side of the data analysis window. Because of the resulting spike at one end of the segment, a straight line through the end points would not reflect the general trend.

In practice, the distorting effect of such a dike can be minimized by using segments shorter than the window size and averaging variograms for several segment positions along-line within the same window.

### CONCLUSION

Assuming self-similar source distributions, I have derived variogram statistical models for  $\Delta T$  magnetic and  $g_z$  gravity data. Variogram models of horizontal and vertical gradiometer data could be found in a similar way.

Statistical features of  $\Delta T$  line data are attributed to four parameters: (1) orientation of profiles relative to the direction of the main field, (2) intensity  $c_s$ , (3) scaling exponent  $\beta$ , and (4) depth  $z$  of source. I developed this model to decompose aeromagnetic surveys into maps of  $c_s$ ,  $\beta$ , and  $z$ , with the highest possible accuracy and resolution. The intensity  $c_s$  can be mapped from single flight lines using a very small window if  $z$  is substituted by the survey terrain clearance and  $\beta$  is kept constant (Maus et al., 1999, this issue, Figure 7). Such high-resolution maps of  $c_s$  are easier to interpret than  $\Delta T$  maps and can therefore be an attractive way of presenting magnetic data. Basement topography can be estimated keeping  $\beta$  constant and  $c_s$  and  $z$  variable (Maus et al., 1996, 1999, this issue). Variogram analysis can also be used to map  $\beta$ , as proposed by Maus and Dimri (1995b). However, because of the large window required for estimating  $\beta$ , maps of the scaling exponent are blurred and may be of limited practical use.

Apart from these applications, variograms provide space domain statistical models for magnetic and gravity data. Such statistical models should be useful in filtering, gridding, inversion, and other processing techniques.

### ACKNOWLEDGMENTS

I thank Peter Weidelt, Richard Blakely, David Chapin, and Harold Yarger for many helpful comments. Furthermore, I am grateful to Vijay Dimri, Saurab Verma, and Harsh Gupta for enabling my very pleasant and productive stay at NGRI Hyderabad in India, where most of this work was done.

### REFERENCES

- Chapin, D. A., 1996, A deterministic approach towards isostatic gravity residuals—A case study from South America: *Geophysics*, **61**, 1022–1033.
- Cressie, N. A. C., 1993, *Statistics for spatial data*: John Wiley & Sons, Inc.
- Gradtsteyn, I. S., and Ryzhik, I. M., 1994, *Table of integrals, series, and products*: Academic Press Ltd.
- Gregotski, M. E., Jensen, O. G., and Arkani-Hamed, J., 1991, Fractal stochastic modeling of aeromagnetic data: *Geophysics*, **56**, 1706–1715.
- Kolmogorov, A. N., 1941, Local structure of turbulence in an incompressible fluid at very high Reynolds numbers: *Dokl. Akad. Nauk SSSR*, **30**, no. 4, 299–303.
- 1961, Local structure of turbulence in an incompressible fluid at very high Reynolds numbers (English translation), *in* Friedlander, S. K., and Topper, L., Eds., *Turbulence. Classical papers on statistical theory*: Interscience, 151–155.
- Mandelbrot, B. B., 1983, *The fractal geometry of nature*: W. H. Freeman & Co.
- Maus, S., 1996, Scaling statistical analysis of magnetic and gravity data: 66th Ann. Internat. Mtg., Soc. Expl. Geophys., Expanded Abstracts, 1419–1421.
- Maus, S., and Dimri, V. P., 1994, Scaling properties of potential fields due to scaling sources: *Geophys. Res. Lett.*, **21**, 891–894.
- 1995a, Basin depth estimation using scaling properties of potential fields: *J. Ass. Expl. Geophys.*, **16**, 131–139.

- 1995b, Potential field power spectrum inversion for scaling geology: *J. Geophys. Res.*, **100**, 12605–12616.
- 1996, Depth estimation from the scaling power spectrum of potential fields?: *Geophys. J. Internat.*, **124**, 113–120.
- Maus, S., Gordon, D., and Fairhead, J. D., 1997, Curie-temperature depth estimation using a self-similar magnetization model: *Geophys. J. Internat.*, **129**, 163–168.
- Maus, S., Green, C. M., and Fairhead, J. D., 1998, Improved ocean geoid resolution from retracked ERS-1 satellite altimeter waveforms: *Geophys. J. Internat.*, **134**, 243–253.
- 1999, Variogram analysis of helicopter magnetic data to identify paleochannels of the Omaruru River, Namibia: *Geophysics*, **64**, 784–793.
- Maus, S., Sengpiel, K. P., and Tordiffe, E. A. W., 1996, Variogram analysis of magnetic data to identify paleochannels of the Omaruru River in Namibia: 66th Ann. Internat. Mtg., Soc. Expl. Geophys., Expanded Abstracts, 1381–1383.
- Naidu, P. S., 1968, Spectrum of the potential field due to randomly distributed sources: *Geophysics*, **33**, 337–345.
- Pilkington, M., and Todoeschuck, J. P., 1990, Stochastic inversion for scaling geology: *Geophys. J. Internat.*, **102**, 205–217.
- 1993, Fractal magnetization of continental crust: *Geophys. Res. Lett.*, **20**, 627–630.
- 1995, Scaling nature of crustal susceptibilities: *Geophys. Res. Lett.*, **22**, 779–782.
- Pilkington, M., Todoeschuck, J. P., and Gregotski, M. E., 1994, Using fractal crustal magnetization models in magnetic interpretation: *Geophys. Prosp.*, **42**, 677–692.
- Spector, A., and Grant, F. S., 1970, Statistical models for interpreting aeromagnetic data: *Geophysics*, **35**, 293–302.
- Yaglom, A. M., 1986, *Correlation theory of stationary and related random functions*, **1**: Springer-Verlag New York, Inc.